APPLIED MATHEMATICS AND WAVEFIELD INVERSION: COMBINING PHYSICAL INSIGHT AND SIMPLE THEORETICAL DEVICES

D. Lesselier[†,*]**, M. Lambert**[†]**, A. Wirgin**[‡]
[†]Département de Recherche en Electromagnétisme - Laboratoire des Signaux et Systèmes (CNRS-Supélec-UPS), France
[‡]Laboratoire de Mécanique et d'Acoustique (CNRS), France
[*]Email: lesselier@lss.supelec.fr

Abstract

Wavefield inversion often involves challenging mathematical problems which are not necessarily prone to obvious solutions, though the complexity of the environment in which the objects (scatterers, sources) to be characterized via wavefield inversion lie, and the complexity of the objects themselves, are such that even high-end models of the real world may remain far too simple. On the other hand, it is necessary to devise solution algorithms the computational level of which should ideally authorize an end-user almost on-line decisions, which might imply more modest goals (distinguishing the few main features of some equivalent simplified object), using modest means, than those initially aimed at. Here, recently or presently developed methods (where physical insight and proper mathematical modeling are combined) are sketched, numerical examples given on common test configurations, and their pros and cons discussed in order to illustrate the above argumentation.

Introduction

The aim of this contribution is to show that non-linearized inversion tools of time-harmonic wavefields which behave quite suitably in simple yet not necessarily canonical configurations of scatterers can be built upon rather low-key theoretical analyses of the scattering phenomenon. By the above, is meant that these tools evidently require a good blend of appropriate theoretical investigations and proper physical insight, but do not impose upon us the burden of too sophisticated mathematics, and more importantly do not suffer too much from discrepancies between the numerical framework effectively put into force and the formal apparatus behind it, or from the lack of proper proofs regarding usual and difficult questions, such as uniqueness and stability.

The material is based upon research results obtained during the last few years by the authors and their co-workers, mostly in acoustics but also in electromagnetics (in cases which may be of relevance to the acoustical community), their main purpose being to illustrate the above argumentation in good fashion. The present contribution focuses on wavefield inversion tools which aim at the identification of the location, the cross-sectional shape and (for penetrable cases) the acoustic parameters of passive 2-D scattering obstacles which are buried in some prescribed free space or layered environment and which are illuminated by a known, possibly frequency-diverse and orientation-diverse primary field.

Only the retrieval of binary objects is considered herein, the said objects consisting of homogeneous zones separated by well defined yet geometrically unknown boundaries, the parameters of the homogeneous zones with respect to the embedding space being either known beforehand or being sought –this notion of binary objects is encompassing here both impenetrable objects (Neumann or Dirichlet boundary condition) and penetrable ones (transmission boundary condition) as well. Four binary-specialized methods investigated by the authors and co-workers, the controlled evolution of level-sets [1], [2], [3], [4], the distributed source method [5], the Intersecting Canonical Body Approximation (ICBA) method [6], [7], [8], and the Modified Rayleigh Conjecture (MRC) method [9], are discussed below, illustrative numerical results given, and possibly needed complementary developments pointed out.

In relation to the topic, it is opportune to mention three recently edited special sections in which the reader may find complementary material contributed by the authors, and many others, with regard to practical, real-world situations: confrontation of a number of linearized and non-linearized inversion algorithms to the same sets of laboratory-controlled microwave data [10], underwater acoustics [11], and nondestructive evaluation of artificial materials [12].

The solution methods

The main model ingredients

Let $u^i(\mathbf{x},\omega)$ be an incident monochromatic wavefield (the $\exp(-j\omega t)$ time (t) factor, with ω the angular frequency, is henceforth implicit) at point $\mathbf{x}=(r,\theta)$ of the xOy plane (i.e., the field that exists in the absence of the object in a medium with some constant wavenumber k), $u^s(\mathbf{x},\omega)$, $u(\mathbf{x},\omega)(=u^i(\mathbf{x},\omega)+u^s(\mathbf{x},\omega))$ the scattered and total fields in response to u^i, Ω being the cross-section of the object within a prescribed search box $\mathcal{D}$ of the xOy plane —Ω is non-necessarily singly-

connected, i.e., there may be several objects in the domain of study—, and $\Gamma = \partial\Omega$ the boundary of the object (or its constitutive parts), assumed to be smooth (C^2-type). If there exists only a single object, the latter is assumed to be representable by the parametric equation $r = \gamma(\theta)$, γ a continuous, single-valued function of θ, the origin being taken at O assumed interior to Ω. Only linear, isotropic, time-invariant materials are considered, fluid ones in acoustics (only compression waves are supported), non-magnetic Maxwellian ones in electromagnetics.

As indicated above, the case under study is binary: the object is made of a homogeneous material and is imbedded in a homogeneous space (for several of the considered methods, it is possible for the host to be horizontally-layered provided the object boundary does not intersect any interface). Two configurations are of interest thereafter, the impenetrable one and the penetrable one.

We illustrate the analysis of the first configuration with acoustically-soft objects, for which a Dirichlet boundary condition holds –with the controlled evolution of level sets, in numerical practice, one simply inputs a high attenuation inside the object domain such that the field cancels out very quickly from the surface inwards due to a strong skin effect. For the analysis of the second configuration, one considers fluid media characterized by their speed of sound (density is assumed constant throughout space, this may not be a minor approximation), which leads to a binary problem in which the ratio (it may be complex-valued, with positive imaginary parts, if losses exist inside the object) between wave numbers k_Ω inside and k outside the object is taken as a constant (prescribed or sought).

The controlled evolution of level sets

This method applies both to penetrable objects and, asymptotically at least, to impenetrable objects (by giving to k_Ω a high imaginary part as indicated above), possibly multiply-connected, and set in free or layered space. It is based on a combination of two methods, the level set representation of shapes [13] and the speed method [14], and allows topological identification in the sense that merging, division, emergence and disappearance of the sought domains are enabled. Indeed, the closed contours Γ of any object are the zero-level of a level set ϕ, and these contours are simply evolved in space $\mathbf{x}$ and pseudo-time t, as a consequence of the evolution of the whole level set, in order that a suitable objective function, $J_\mathcal{M}$, be minimized. The latter function basically (since one could further impose constraints of least perimeters and least areas) is made of the mean square norm of the discrepancy between the scattered field effectively collected in some exterior-to-$\mathcal{D}$ measurement domain, $\mathcal{M}$, and the one associated with an object retrieved within $\mathcal{D}$ at a given t with contour(s) Γ_t, appropriately normalized with respect to the mean square norm of the data.

The evolution itself is governed by a Hamilton-Jacobi (HJ) equation which links, through the action of the velocity field of motion (oriented along $\mathbf{n}$ the unit normal to the contour Γ_t, with algebraic value V), the partial derivative of ϕ with respect to t to the norm of its gradient in space: $\frac{\partial\phi}{\partial t}(\mathbf{x},t) + V(\mathbf{x},t)\,|\nabla\phi(\mathbf{x},t)| = 0, \forall \mathbf{x} \in \mathcal{D}, \forall t \geq 0$.

The velocity V is now built so that the derivative $\mathrm{d}J_\mathcal{M}/\mathrm{d}\,t$ of the objective function with respect to time is negative (pending numerical uncertainties). It can be shown, within a rigorous Green domain integral framework of the wavefield and using appropriate elements of control theory, that $V(\mathbf{x},t) = -\Re[g(\mathbf{x},t)]$, where g is the so-called shape gradient at Γ_t, extended to all points inside $\mathcal{D}$, the latter being proportional to $[u(\mathbf{x})p(\mathbf{x})]$; p is an adjoint field whose source term is made as is usual from the conjugated discrepancy of the data error in $\mathcal{M}$ and which satisfies domain integral equations similar to those satisfied by u.

The above results being available, a fast marching algorithm, via discretization in time (step Δt) and space (with fixed grid), of the HJ equation yields, from a given level set ϕ at $n\Delta t$ and a given velocity, an updated level set one time step ahead, at $(n+1)\Delta t$; its zero level yields the newly retrieved boundary, and a new velocity follows from the shape gradient calculated by solving the corresponding direct and adjoint problems. This goes on until a satisfactory solution is obtained (with hopefully low data error in $\mathcal{M}$). It should be emphasized that the object boundary is implicit (black, non-zero-contrast pixels inside it and white, zero-contrast pixels outside it provide the map of Ω_t).

When contrast and shape are both unknown, one simply resorts to a sequence of optimal searches, one via the above procedure for a given contrast, one for a given shape, via a Levenberg-Marquardt non-linear solver as is summarized in [4], numerical experimentation guiding us to select the best parameters for each optimization.

The distributed source method

This method applies to a single, acoustically-soft or acoustically-hard, object, which is star-shaped with respect to the origin of coordinates (assumed to be a reference interior point). It involves the minimization of a two-term objective functional $J_\mathcal{M} + \sigma J_\Gamma$ with real positive weighting parameter σ; the first term $J_\mathcal{M}$, as before, contains the fit in $\mathcal{M}$ between data and field associated to the test object, and the second term J_Γ is associated to the satisfaction of the boundary condition

on its contour.

Henceforth assuming a test object with contour Γ described by function $\gamma(\theta)$, the scattered field at $\mathbf{x}$ is equated to a finite weighted sum of M exact Green functions of the unperturbed (free or layered) environment, $G(\mathbf{x}, \mathbf{x}_m^\Gamma)$. Their source locations $\mathbf{x}_m^\Gamma, m = 1, .., M$, are on a closed curve $\hat{\Gamma}$ kept inside the domain encircled by Γ and homothetic with it, by enforcing $\left|\mathbf{x}_m^\Gamma(\theta)\right| = \alpha\gamma(\theta)$, α constant real multiplicative factor less than 1. One thus has $u^s(\Gamma, \mathbf{x}) = \sum_{m=1}^M c_m G(\mathbf{x}, \mathbf{x}_m^\Gamma)$, which corresponds to a truncation of an infinite series made of Green's functions with position-independent weighting coefficients (complete family representation). Correspondingly, the boundary cost function, J_Γ, is the normalized mean square norm of the error along Γ in canceling out either the total field (Dirichlet) or its normal derivative (Neumann); the normalization is now carried out with respect to the norm of the incident field u^i at the same location, or of its normal derivative.

In practice, the boundary condition is enforced at Q discrete nodes chosen at regularly spaced angles θ_q, and the Dirichlet hypothesis leads to $J_\Gamma = \sum_{q=1}^Q |u(\Gamma, \theta_q)|^2 J_{a\Gamma}(\theta_q) / \sum_{q=1}^Q \left|u^i(\Gamma, \theta_q)\right|^2 J_{a\Gamma}(\theta_q)$; here, $u(\Gamma, \theta_q)$ (resp., $u^i(\Gamma, \theta_q)$) is the total (resp., incident) field at point γ_q $(= \gamma(\theta_q), \theta_q)$, and $J_a(\theta_q)$ is the discrete value of the Jacobian $J_{a\Gamma}(\theta) = (\gamma^2 + (\frac{d\gamma}{d\theta})^2)^{\frac{1}{2}}$, the Jacobian transformation enabling to calculate the boundary cost function on the fixed unit circle and not on the evolved contour. As for the Neumann hypothesis, it is dealt with by replacing u by $\partial_n u$ in the above Dirichlet-type equation. The object contour Γ is easily described by means of a $2N$-coefficient sine-cosine expansion of the function $\gamma(\theta)$.

The unknowns are the $2N$ real coefficients a_n (describing Γ) and the M complex coefficients c_m (amplitudes of the interior sources), the boundary condition being enforced at the Q nodes on Γ. These coefficients are obtained by a Levenberg-Marquardt solution algorithm, starting from an initial shape contour (via the a_n) and an initial field (via the c_m), typically an initial circle: $a_0 = R_0, a_{1,...} = 0$, all equivalent sources being extinguished ($c_m = 0, \forall m$). The limitation of the method is that the contour should be star-like with respect to an inner point, but here, as illustrated in the corresponding numerical example the co-ordinates of the reference point are also considered as being unknown and are provided by the solution algorithm.

Notice that a penetrable object could be retrieved by using two sets of equivalent sources (inside, to model the outer field, outside, to model the inner field), transmission conditions being enforced on the sought contour, like in the earlier investigation [15], but this mostly remains to be probed further.

The ICBA and MRC methods

Let us henceforth consider an acoustically-soft, singly-connected object in free space. The Modified Rayleigh Conjecture (MRC) enables us to obtain the partial wave amplitudes directly from the scattered field, collected on a circle completely enclosing the object, and then to obtain the shape by use of the Rayleigh hypothesis ansatz of the scattered field [6] in the boundary condition. Let Γ_b be a circle of radius b that circumscribes the object, the origin O being assumed somewhere within it, with $b > \overline{\gamma} := \max_{\theta \in [0, 2\pi[} \gamma$, where the scattered field, $\hat{u}^s$, is collected. The contour function $\gamma(\theta)$ which embodies all that is known about the object is arrived at as follows.

The partial circular cylindrical wave representation is $u(\mathbf{x}) = u^i(\mathbf{x}) + \sum_{n=-\infty}^{\infty} A_n H_n^{(1)}(kr) e^{jn\theta}, r \geq \overline{\rho}, \theta \in [0, 2\pi[$, wherein $H_n^{(1)}$ are the Hankel functions of the first kind and n-th order, and A_n the coefficients that result from a weighted integration of the measured scattered field $\hat{u}^s$ (a corrupted set of data should mostly affect coefficients of large indices, and at the end enable us to reconstruct only a smoothed profile). The Rayleigh hypothesis (termed "conjecture" in [16], [17]) now assumes that the cylindrical wave representation approximately holds up to the boundary of the object. The Rayleigh coefficients A_n^R are to be used instead of the A_n and summed from $n = -N$ to N, those A_n^R being henceforth taken as $\approx A_n, \forall n \in [-N, N]$.

Field cancellation on the boundary means that $u^i(\gamma(\theta), \theta) + \sum_{n=-N}^{N} A_n^R H_n^{(1)}(k\gamma(\theta)) e^{jn\theta} \approx 0, \theta \in [0, 2\pi[$. A discrete form, $\gamma_m := \gamma(\theta_m), m = 1, .., M$ of the actual boundary Γ follows by searching for the minima of the set of M uncoupled nonlinear cost functions $J(\gamma_m, \theta_m) := \left|u^i(\gamma_m, \theta_m) + \sum_{n=-N}^{N} A_n^R H_n^{(1)}(k\gamma_m) e^{jn\theta_m}\right|^2$, $m = 1, .., M$. As an alternative, one can expand the contour function into a Fourier series as previously, and seek its Fourier coefficients via minimization of a coupled set of cost functions.

The uncoupled version of the MRC procedure (employed herein) is close to, and the numerical effort is about the same as with, the ICBA method [7]. But key differences remain. In the ICBA method, for any particular scattering direction, the measured field is considered to be none other than the one due to a canonical object, here a circular disk, of same material composition and illuminated by the same incident field.

The field scattered by such a disk satisfies a relationship of the form $u(\mathbf{x}) \approx u^i(\mathbf{x}) + \sum_{n=-\infty}^{\infty} B_n(\gamma(\theta)) H_n^{(1)}(kr) e^{jn\theta}, r \geq \overline{\gamma}, \theta \in [0, 2\pi[$ where the B_n coefficients are known in closed form

for a given radius and a given contrast. Each radius γ_m of the locally equivalent disk at θ_m is found by minimizing the non-linear cost function $K(\gamma_m, \theta_m) := \left|u^s(b,\theta_m) - \sum_{n=-N}^{N} B_n(\gamma_m) H_n^{(1)}(kb) e^{jn\theta_m}\right|^2$, and the discretized contour of the object follows from the minima of the uncoupled set of cost functions $\{K(\gamma_m, \theta_m);\ m = 1, 2, .., M\}$. If the contrast is itself unknown, one may solve the set of now coupled non-linear equations at once. Dealing with the Fourier coefficients of the contour function is also an option.

Both the MRC and ICBA methods require a suitable field expansion of order N (like $\approx k\overline{\gamma}$) –which fail to correctly describe the scattered field if the sought object is needle-like, exhibits strong concavities (the distributed source method would fail as well), or is largely-decentered with respect to the origin O of the laboratory frame– call for commensurate Fourier expansion of the contour (if it is employed) and a Rayleigh-type expansion of the field, while suffering from non-uniqueness of the solutions even in ideal cases.

In short, the two methods call for a suitable (although fully-automated) post-processing (called 'proximity of minima positions') scheme to get the most plausible contour (using data at two or even more frequencies, the sought boundary being expected to be the only one that moves the least with frequency as is discussed in [9]).

An interesting feature of the ICBA method is that it readily applies to a penetrable object and even layered environments can be considered as long as some canonical object scatters off a field which is known in suitably simple closed form [11]) and can be used locally to match to the sought one, with no theoretical worries of the kind met with the MRC.

Numerical illustrations

In the following, the first two solution methods (controlled evolution of level sets and the distributed sources) are tested against synthetic data obtained by solving the boundary integral equations rigorously satisfied by the wave field using a method of moments. As for the two other methods under evaluation, the ICBA solution method is tested against data generated by the Rayleigh hypothesis technique, and the MRC solution method is tested against data generated by the ICBA.

The configuration under study consists of a single square obstacle of size $a = 0.888$ mm centered at $(x = 0.25\text{ mm}, y = 0.25\text{ mm})$ which can be penetrable (sound speed $c = 1800$ m/s and attenuation $\alpha = 0$), or sound-soft (Dirichlet boundary condition), and which is embedded in water (sound speed $c_{\text{water}} = 1470$ m/s and attenuation $\alpha_{\text{water}} = 0$) —attenuation if any is introduced through the wave number k as $k = 2\pi f/c + \mathrm{i}\alpha$ where f is the frequency. Density is fixed everywhere to $\rho = 1$.

The illumination then may consist of four line sources at four frequencies (0.5, 1.0, 1.5 and 2.0 MHz) placed each $\pi/2$ on a 3 mm-radius circle, 32 receivers each $\pi/16$ on the 3 mm-radius circle collecting the scattered field for each probe wave, and all such data being employed simultaneously in the inversion. This is the case with the first two solution methods.

As for both the MRC and the ICBA methods, four plane probe waves at angles $\theta^i = 0, \pi/2, \pi, 3\pi/2$ are considered, and, since these methods reconstruct the boundary in a local manner, the dataset associated to $\theta^i = 0$ is employed to retrieve the boundary in the angular sector $-\pi/4 < \theta < \pi/4$, the one associated with $\theta^i = \pi/2$ is employed to get the boundary in the next angular sector $\pi/4 < \theta < 3\pi/4$, and so on. Now, only two frequencies, either 0.5 and 1.2 MHz (low-frequency pair), or 2.3 and 2.5 MHz (high-frequency pair) are used.

Let us emphasize also that the results obtained by the method of controlled evolution (with or without contrast reconstruction) are obtained using a search zone of 2.5 mm $\times$ 2.5 mm centered at $(x = 0\text{ mm}, y = 0\text{ mm})$ and discretized into 40×40 pixels, whereas those obtained by the MRC and ICBA only assume that the obstacle is located within the much larger disk of radius 3 mm defined by the receivers, the origin of the reference frame being then assumed to be contained within the obstacle.

Penetrable obstacle

In figure 1 are presented the results obtained by the method of controlled evolution combined with the contrast reconstruction. The process is initialized with a single square obstacle (figure 1(a)) of sound-speed $c = 2000$ m/s. The best solution (corresponding to the lowest value of the cost function) is presented in figure 1(b). The cost function and contrast evolutions as a function of the iteration number are depicted in figure 1(c) and figure 1(d), respectively. The reconstructed obstacle (obtained at iteration 23) perfectly fits the exact one and its sound-speed is found to be equal to 1799.38 m/s.

Impenetrable obstacle

As indicated below, the reconstruction of an impenetrable obstacle by the method of controlled evolution as introduced here is not straightforward. As a matter of fact the evolution of the obstacle contour during the iterative procedure is proportional to the total field: the interior total field of an impenetrable obstacle is zero, which does not allow any evolution. So, one introduces some large attenuation allowing a limited field penetra-

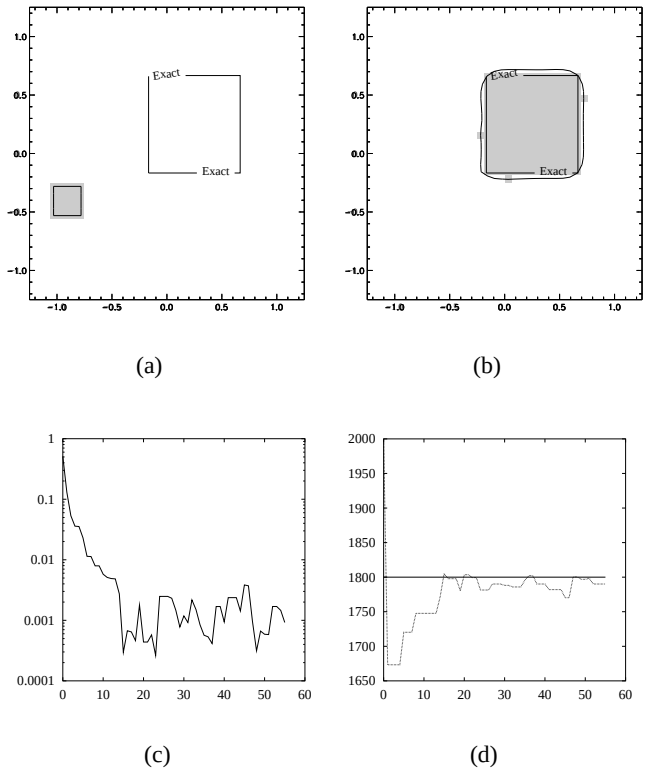

Figure 1: Reconstruction of a penetrable obstacle by controlled evolution of level sets with contrast optimization: initialization ($c = 2000$ m/s) (a), the best reconstruction (iteration 23) (b), evolution of the cost function as a function of the number of iterations (c) and the one of the sound speed of the obstacle (d).

tion in the obstacle. The idea is to use a set of increasing attenuations so as to lead to a progressively-improved description of the boundary. In our example (figure 2) one uses $\alpha = 10^3, 3\ 10^3$ and $6\ 10^3$. The procedure (figure 2(a)) is initiated with the lowest attenuation. Once convergence is observed, the best solution reached at that point is taken as the initial solution with a higher attenuation (here $\alpha = 3\ 10^3$). And so on, until convergence. In figure 2(e) is illustrated the convergence of the procedure with respect to the different attenuations chosen.

The results obtained by the distributed source technique are presented in figure 3. The reconstructions are obtained using $M = 30$ and $N = 4, 8$; note that the center (x, y) of the star-like shape has not been fixed beforehand and is searched also. The procedure is initialized by a circular test obstacle of radius $r = 0.5$ mm centered at $(x = 0, y = 0)$. Then the sought boundary is described using a small number of coefficients a_n (here $n = 1, \ldots, 2N(= 8)$) to constrain the boundary to remain smooth. Upon convergence the number of coefficients is increased ($n = 1, \ldots, 2N(= 16)$), using the final solution of the first inversion as initial guess.

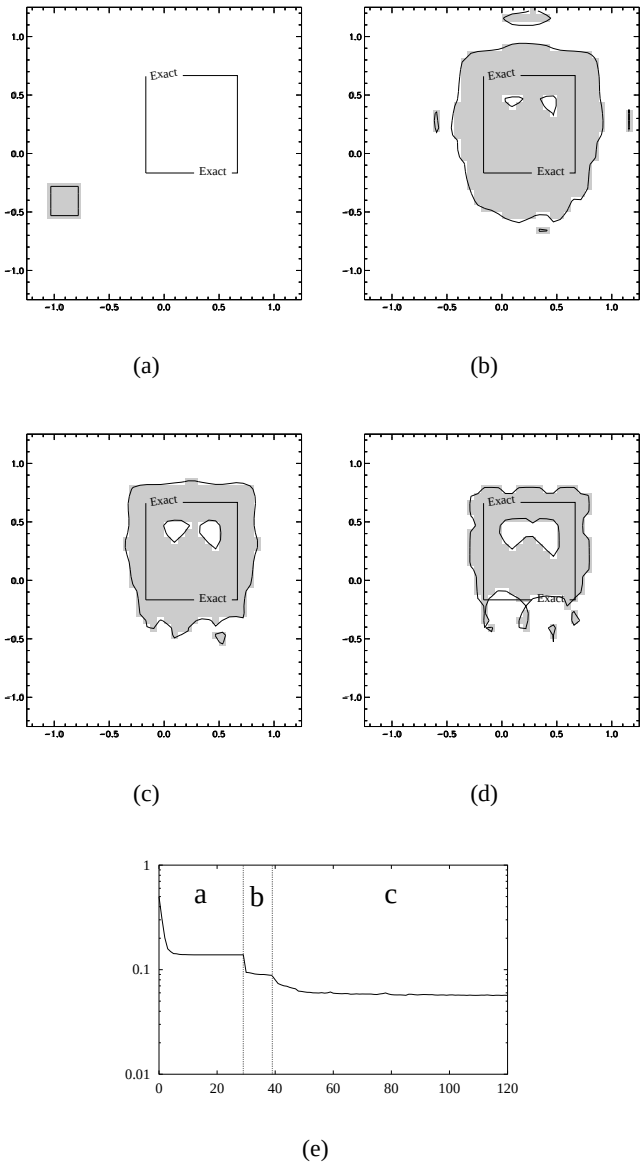

Figure 2: Reconstruction of a sound-soft obstacle by controlled evolution of level sets with fixed contrast: initialization ($\alpha = 10^3$) (a), the best solution obtained with $\alpha = 10^3$ (b), with $\alpha = 3\ 10^3$ (c) and with $\alpha = 6\ 10^3$ (d), evolution of the cost function as a function of the number of iterations (e).

In figure 3(a) the first-guess obstacle compared to the exact one and the best solution which is reached with $N = 4$ coefficients are shown. In figure 3(b) the best solution reached with $N = 8$ coefficients is shown, the procedure being started from the previous $N = 4$ solution.

For the ICBA and MRC solution methods, since they work in similar fashion, they are illustrated together. For each probe radiation frequency f and each discrete polar angle θ, a set of candidate solutions (minima, both global and relative, of the cost function expressing the discrepancy between the data and the estimator thereof

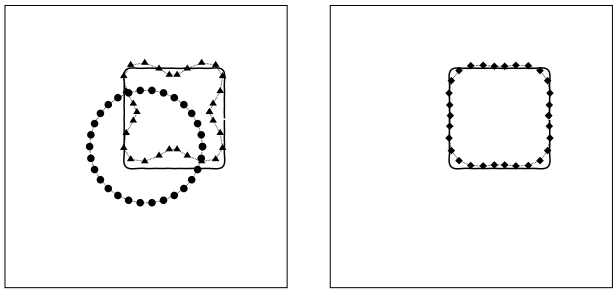

(a) (b)

Figure 3: Reconstruction of a sound-soft obstacle using the distributed source method. (a) $N = 4$: initialization (●), the best solution (▲, iteration 300); (b) $N = 8$: the best solution (◆, iteration 100).

for trial boundaries) is given. Both candidate boundary points at each frequency of operation (specified by 'o' for the lower frequency and by 'x' for the higher frequency in the same pair) and post-processed boundary points are depicted. The goal of the post-processing is to single out a unique solution for each angle θ in searching (by 'proximity analysis') for the two points in the above two sets that are closest to each other (since theory suggests that two points of these two sets that are coincident designate the correct boundary point). This is done in fully-automatic (no human intervention) manner by the computer —ideally, the reconstructed boundary should appear as a set of points, each one of which is the coincident location of a 'o' and 'x' for each θ_m.

Figs. 4-5 pertain to the reconstructions obtained by the ICBA method, using the low- and high-frequency pairs, the boundary being recovered fairly accurately for both.

Figs. 6-7 pertain to the reconstructions obtained by the MRC method, using the low- and high-frequency pairs. One observes that the boundary is not well-recovered, especially for the lower-frequency probe radiation pair. The fact that the results are quite different in the low- and high-frequency regimes may be an indication of the instability of this method, notably at the stage whereby the Rayleigh coefficients are obtained by quadrature of the data. Notice should be taken of the fact that if the search zone had been made smaller (as for the level-set and distributed source methods), many of the spurious solutions in Figs.6-7 would have been eliminated.

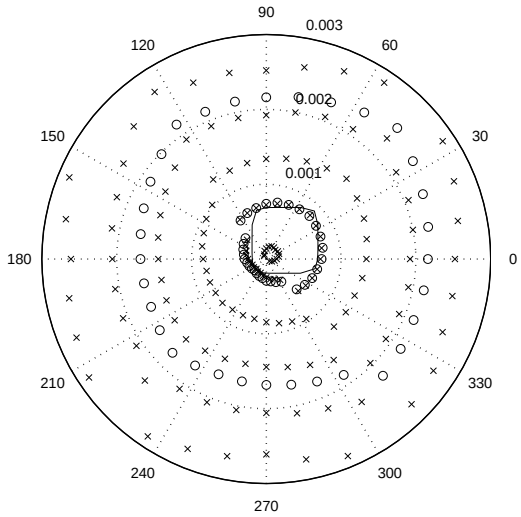

(a)

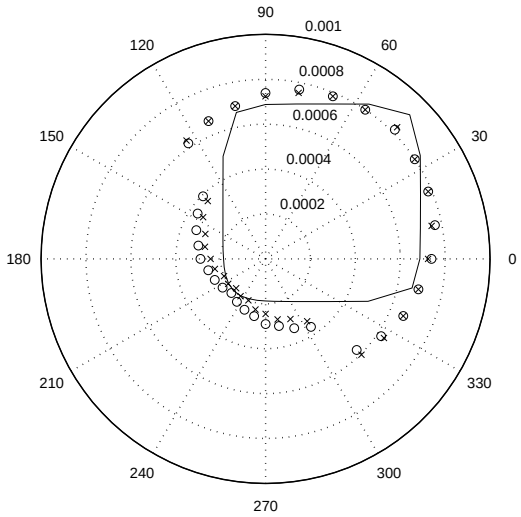

(b)

Figure 4: ICBA method: (a) Candidate solutions with the low-frequency pair: 0.5 MHz ('o'), 1.2 MHz ('x'). Actual boundary: full curve. (b) Results of the proximity analysis (same symbols).

References

[1] C. Ramananjaona, M. Lambert, D. Lesselier, and J.-P. Zolésio, "Shape reconstruction by controlled evolution of a level set: from a min-max formulation to numerical experimentation," Inverse Probl., vol. 17, pp. 1087-1111, 2001. Corrigendum, vol. 17, pp. 2017-2022, 2001.

[2] C. Ramananjaona, M. Lambert, and D. Lesselier, "Shape inversion from TM and TE real data by controlled evolution of level sets," Inverse Probl., vol. 17, pp. 1585-95. Corrigendum, vol. 18, pp. 279-282, 2002.

[3] C. Ramananjaona, M. Lambert, D. Lesselier, and J.-P. Zolésio, "On novel developments of con-

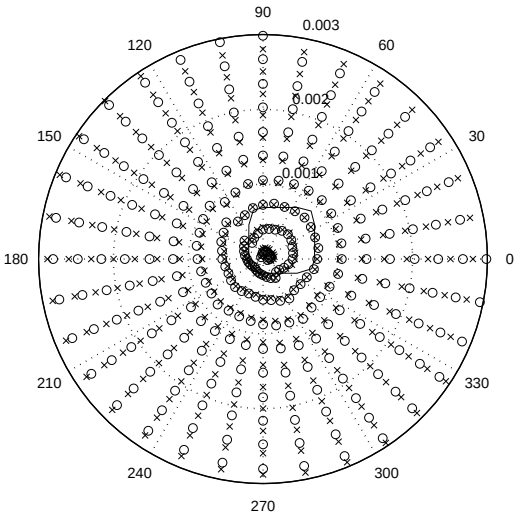

(a)

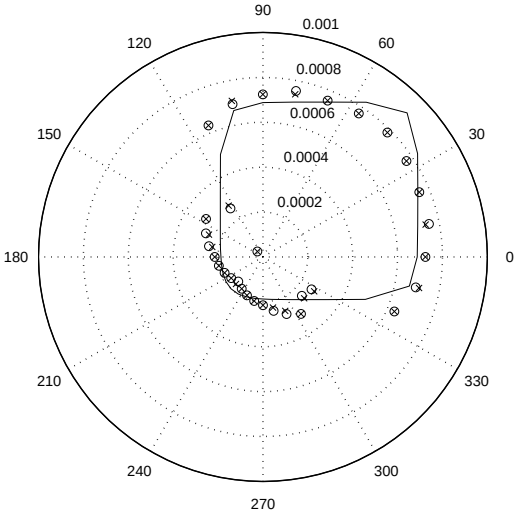

(b)

Figure 5: ICBA method: (a) Candidate solutions as in Fig. 4 but with the high-frequency pair at 2.3 and 2.5 MHz. (b) Results of the proximity analysis (same symbols).

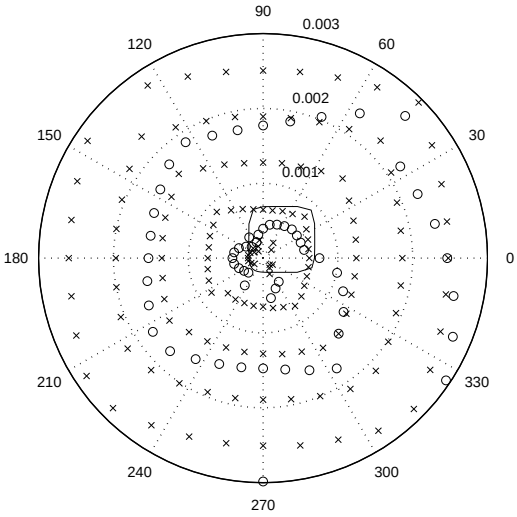

(a)

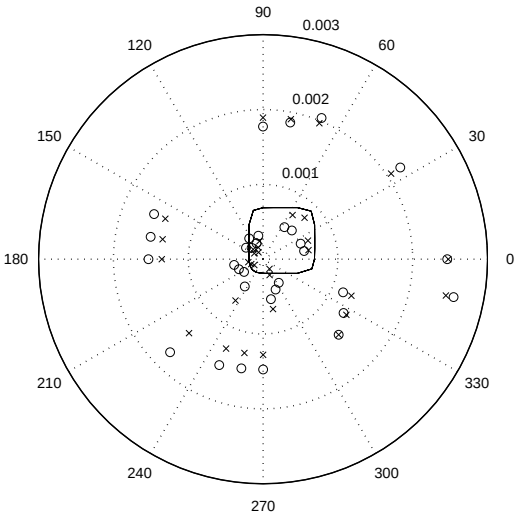

(b)

Figure 6: MRC method: (a) Candidate solutions with the low-frequency pair: 0.5 MHz (‘o’), 1.2 MHz (‘x’). Actual boundary: full curve. (b) Results of the proximity analysis (same symbols)

trolled evolution of level sets in the field of inverse shape problems,” Radio Sci., vol. 37, doi:10:1029/2001RS002567, 2002. [printed vol. 38, pp. VIC 11-1-VIC-11-9, 2003]

[4] —, “On the controlled evolution of level sets and like methods: the shape and contrast reconstruction,” in Acoustics, Mechanics, and the Related Topics of Mathematical Analysis, A. Wirgin ed., World Scientific, Singapore, 2002, pp. 243-250.

[5] M. Lambert and D. Lesselier, “Distributed source method for retrieval of the cross-sectional contour of an impenetrable cylindrical object in a shallow water waveguide,” ACUSTICA - Acta Acustica, vol. 86, pp. 15-24, 2000.

[6] T. Scotti and A. Wirgin, “Shape reconstruction of an impenetrable scattering body via the Rayleigh hypothesis,” Inverse Probl., vol. 12, pp. 1027-1055, 1996.

[7] E. Ogam, T. Scotti, and A. Wirgin, “Non-ambiguous boundary identification of a cylindrical object by acoustic waves,” C. R. Acad. Sci. IIb,

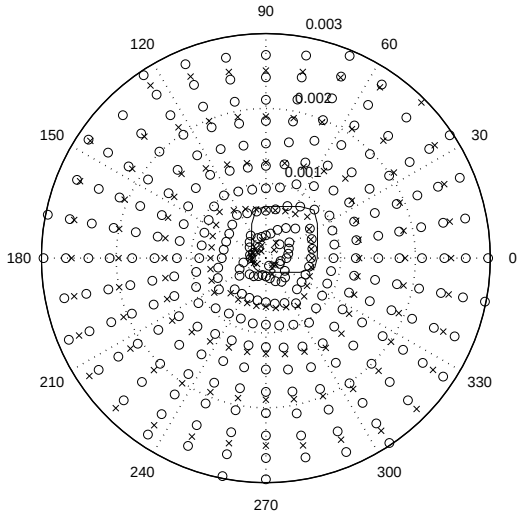

(a)

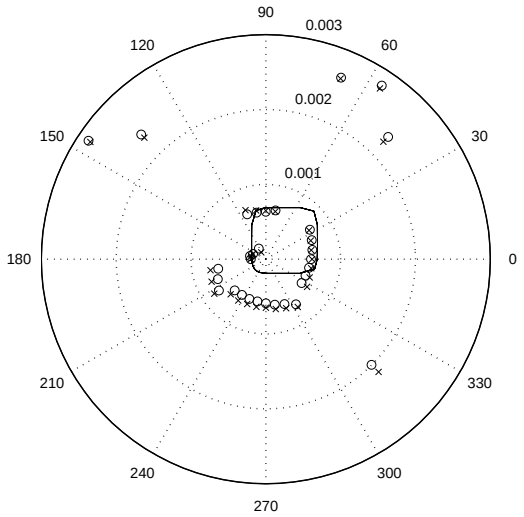

(b)

Figure 7: MRC method: (a) Candidate solutions as in Fig. 6 but with the high-frequency pair at 2.3 and 2.5 MHz. (b) Results of the proximity analysis (same symbols)

vol. 329, pp. 61-66, 2001.

[8] —, "Non-uniqueness in connection with methods for the reconstruction of the shape of cylindrical bodies from acoustic scattering data," in Acoustics, Mechanics, and the Related Topics of Mathematical Analysis, A. Wirgin ed., World Scientific, Singapore, 2002, pp. 222-228.

[9] A. Wirgin, "Use of the Modified Rayleigh Conjecture method for determining the shape of an acoustically-soft bounded 2D body from the scattered field," Int. J. Applied Electromagn. Mechan., to appear, 2004.

[10] Special Section on Testing Inversion Algorithms against Experimental Data, K. Belkebir and M. Saillard ed., Inverse Probs., vol. 17, pp. 1565-1701, 2001.

[11] Special Section on Underwater Acoustics, A. Wirgin ed., Inverse Probs., vol. 17, pp. 1619-1811, 2001.

[12] Special Section on Electromagnetic and Acoustic nondestructive Evaluation, D. Lesselier and J. Bowler ed., Inverse Probs., vol. 19, pp. 1733-1958, 2003.

[13] J.A. Sethian, Level Set Methods and Fast Marching Methods 2nd ed., Cambridge Univ. Press, Cambridge, 1999.

[14] J. Sokolowski and J.-P. Zolésio, Introduction to Shape Optimization. Shape Sensitivity Analysis, Springer-Verlag, Berlin, 1992.

[15] Y. Leviatan and Y. Meyouhas, "Analysis of electromagnetic scattering from buried cylinders using a multifilament model," Radio Sci., vol. 25, pp. 1231-1244, 1990.

[16] A.G. Ramm, "Modified Rayleigh conjecture and applications," J. Phys. A, vol. 35, pp. L357-L361, 2002.

[17] S. Gutman and A.G. Ramm, "Numerical implementation of the MRC method for obstacle scattering problems," J. Phys. A, vol. 35, pp. 1-11, 2002.

Acknowledgements

The controlled evolution of level sets as is discussed herein owes much to the work of C. Ramananjaona and J.-P. Zolésio.